

draft version April 21, 2018,

## The influence of inelastic neutrino reactions with light nuclei on the standing accretion shock instability in core-collapse supernovae

Shun Furusawa<sup>1</sup>, Hiroki Nagakura<sup>1,2</sup>, Kohsuke Sumiyoshi<sup>3</sup> and Shoichi Yamada<sup>1,4</sup>

furusawa@heap.phys.waseda.ac.jp

### ABSTRACT

We perform numerical experiments to investigate the influence of inelastic neutrino reactions with light nuclei on the standing accretion shock instability (SASI). The time evolution of shock waves is calculated with a simple light-bulb approximation for the neutrino transport and a multi-nuclei equation of state. The neutrino absorptions and inelastic interactions with deuterons, tritons, helions and alpha particles are taken into account in the hydrodynamical simulations in addition to the ordinary charged-current interactions with nucleons. Axial symmetry is assumed but no equatorial symmetry is imposed. We show that the heating rates of deuterons reach as high as  $\sim 10\%$  of those of nucleons around the bottom of the gain region. On the other hand, alpha particles are heated near the shock wave, which is important when the shock wave expands and the density and temperature of matter become low. It is also found that the models with heating by light nuclei have different evolutions from those without it in the non-linear phase of SASI. This results is because matter in the gain region has a varying density and temperature and there appear sub-regions that are locally rich in deuterons and alpha particles. Although the light nuclei are never dominant heating sources and they work favorably for shock revival in some cases and unfavorably in other cases, they are non-negligible and warrant further investigation.

### 1. Introduction

The mechanism of core-collapse supernovae is not clearly understood at present because of its intricacy (see e.g. Kotake et al. (2006); Janka (2012); Burrows (2012)). Many numerical

---

<sup>1</sup>Advanced Research Institute for Science and Engineering, Waseda University, 3-4-1, Okubo, Shinjuku, Tokyo 169-8555, Japan

<sup>2</sup>Yukawa Institute for Theoretical Physics, Kyoto University, Oiwake-cho, Kitashirakawa, Sakyo-ku, Kyoto, 606-8502, Japan

<sup>3</sup>Numazu College of Technology, Ooka 3600, Numazu, Shizuoka 410-8501, Japan

<sup>4</sup>Department of Science and Engineering, Waseda University, 3-4-1 Okubo, Shinjuku, Tokyo 169-8555, Japan

simulations performed by different groups have consistently demonstrated that the shock waves formed by the bounce of collapsing cores are decelerated and stalled by the energy losses due to the dissociations of nuclei and emissions of neutrinos. For the moment, the neutrino-heating is considered to be the most promising mechanism of shock revival, in which the neutrinos emitted from the proto-neutron star reinvigorate the stalled shock to propagate outward again, although some other mechanisms, e.g. magneto-rotational explosion, may be needed for very massive stars. It is also believed that the so-called standing accretion shock instability (SASI) and convection are essential to increase the efficiency of neutrino heating (Herant et al. 1992; Burrows et al. 1995; Fryer et al. 2002; Blondin et al. 2003; Fryer 2004; Scheck et al. 2004, 2006; Ohnishi et al. 2006; Foglizzo et al. 2006, 2007, 2012; Iwakami et al. 2008, 2009; Fernández & Thompson 2009a,b; Fernández 2010; Hanke et al. 2012, 2013; Müller et al. 2012; Bruenn et al. 2013; Ott et al. 2013; Murphy et al. 2013). Indeed, it is recently found that multi-D numerical simulations have successfully relaunched the stalled shock wave, which may eventually produce supernova explosions as we see them (Buras et al. 2006a,b; Marek et al. 2009; Suwa et al. 2010, 2011; Müller et al. 2012; Kuroda et al. 2012; Takiwaki et al. 2012; Bruenn et al. 2013; Ott et al. 2013; Murphy et al. 2013). All these simulations are not long enough so far, however, and it is remaining to see if they can really reproduce the canonical explosion energy and  $^{56}\text{Ni}$  mass (Yamamoto et al. 2013). In addition to these hydrodynamical effects, there are some nuclear-physical ingredients that are also supposed to be important for reproducing the core-collapse supernovae. Nuclear burning in the accreting matter and ejecta was investigated by Nakamura et al. (2012) and Yamamoto et al. (2013). The inelastic neutrino interactions as well as the baryonic equation of state (EOS) are also important as described below.

The inelastic interactions between neutrinos and nuclei have been neglected in most hydrodynamical simulations of the neutrino heating. Haxton (1988) was the first to point out the importance of these reactions. O’Connor et al. (2007), Arcones et al. (2008), Langanke et al. (2008) and Barnea et al. (2008) investigated their influences on the dynamics, neutrino spectrum as well as nucleosynthesis. There is, however, no investigation of the impact of the inelastic reactions on multi-D hydrodynamics but Ohnishi et al. (2007). They showed that the inelastic neutrino interactions with alpha particles are helpful to revive the shock in 2D simulations if the neutrino luminosity is close to the critical value, which is the threshold for a shock revival. They took into account only alpha particles as additional heating sources, since the mass fractions of other nuclei were not available in the EOS they used (Shen et al. 1998a,b). However, the shocked matter is certainly composed not only of nucleons and alpha particles but also of deuterons, tritons and helions (Sumiyoshi et al. 2008; Arcones et al. 2008; Hempel et al. 2012). The energy-transfer coefficients, that is, the average values of the product of the cross section and energy transfer of deuterons are comparable to those of nucleons and ten times greater than those of alpha particles (Nakamura et al. 2009). Tritons and helions have also larger energy-transfer coefficients than alpha particles (O’Connor et al. 2007; Arcones et al. 2008; Nakamura et al. 2009).

The EOS is another important physical input in supernova simulations and its influences

on the dynamics of core-collapse supernovae has been investigated by many researchers, e.g. Sumiyoshi et al. (2005), Marek et al. (2009), Hempel et al. (2012), Suwa et al. (2013) and Couch (2013) to mention a few. There are currently two EOS's that are widely used for the simulations: Lattimer-Swesty's EOS (Lattimer et al. 1991) and Shen's EOS (Shen et al. 1998a,b, 2011). In both EOS's, the ensemble of heavy and light nuclei is approximated by a single representative heavy nucleus and alpha particle. In this decade, however, some EOS's that incorporate a large number of nuclei have been constructed (Botvian et al. 2004; Botvina et al. 2010; Hempel et al. 2010; Blinnikov et al. 2011; G. Shen et al. 2011). We have also developed such an EOS (Furusawa et al. 2011, 2013). We employ the liquid drop model for heavy nuclei and take into account shell effects and nuclear pasta phases. Unbound nucleons are treated by the relativistic mean field theory (Furusawa et al. 2011). Moreover, we implement some important improvements such as the inclusion of the Pauli and self-energy shifts in the mass evaluation of light nuclei (Furusawa et al. 2013). As a result, the mass fractions of various light nuclei have become much more reliable.

The aim of this paper is to investigate the impacts of the inelastic neutrino reactions with light nuclei on the SASI based on our new EOS. We perform experimental simulations of the post-bounce phase in 2D, employing the light bulb approximation for neutrino transfer. In addition to the ordinary cooling and heating by nucleons, we incorporate the heating by deuterons, tritons, helions and alpha particles. This article is organized as follows. In section 2, we describe some important ingredients in numerical simulations such as the hydrodynamics code and the rates of inelastic reactions with light nuclei that we employ in this study. Then the results are shown in section 3, with an emphasis being put on the role of light nuclei in the shock heating. The paper is wrapped up with a summary and some discussions in section 4.

## 2. Models

The basic set-up of our dynamical simulations is the same as that given in Ohnishi et al. (2006, 2007) and Nagakura et al. (2013) except for the inelastic reactions with light nuclei. We perform 2D simulations assuming axial symmetry. Spherical coordinates are used and no equatorial symmetry is assumed. We utilize 300 radial mesh points to cover  $r_{in} \leq r \leq r_{out}$  ( $= 500$  km), where  $r_{in}$ , the inner boundary of the computation domain, is set to be the radius of the neutrino sphere of  $\nu_e$  in the initial state. We deploy 60 angular mesh points to cover the whole meridian section. We solve the following equations

$$\frac{d\rho}{dt} + \rho \nabla \cdot \mathbf{v} = 0, \quad (1)$$

$$\rho \frac{d\mathbf{v}}{dt} = -\nabla p + \rho \nabla \left( \frac{GM_{in}}{r} \right), \quad (2)$$

$$\rho \frac{d}{dt} \left( \frac{e}{\rho} \right) = -p \nabla \cdot \mathbf{v} + Q_E + Q_d + Q_t + Q_h + Q_\alpha, \quad (3)$$

$$\frac{dY_e}{dt} = Q_N, \quad (4)$$

where  $\rho$ ,  $p$ ,  $T$ ,  $e$  and  $Y_e$  denote the mass density, pressure, temperature, energy density and electron fraction, respectively. Other symbols,  $r$ ,  $\mathbf{v}$ , and  $G$ , stand for the radius, fluid velocity and gravitational constant, respectively. The mass of a central object,  $M_{\text{in}}$ , is assumed to be constant and set to be  $M_{\text{in}} = 1.4M_{\odot}$ . Interactions between neutrinos and nucleons are encapsulated in  $Q_E$  and  $Q_N$ , the expressions of which are adopted from Eqs. (16) and (17) in Ohnishi et al. (2006).  $Q_{d,t,h,\alpha}$  are the heating rates for the light nuclei indicated by the subscripts. The heating for alpha particles,  $Q_{\alpha}$ , corresponds to  $Q_{\text{inel}}$  in Eqs.(3) and (6) in Ohnishi et al. (2007), where only alpha particles were taken into account as the additional heating source. The heating rates for deuterons, tritons and helions,  $Q_{d,t,h}$ , are the new elements in this work.

The neutrino transport is handled by the simple light bulb approximation, in which neutrinos with Fermi-Dirac distributions are assumed to be emitted from the proto-neutron star and travel radially. We also assume that the temperatures of  $\nu_e$ ,  $\bar{\nu}_e$  and  $\nu_{\mu}$  are constant and set to be  $(T_{\nu_e}, T_{\bar{\nu}_e}, T_{\nu_{\mu}}) = (4, 5, 10)$  in MeV. The luminosities of  $\nu_e$  and  $\bar{\nu}_e$  are assumed to have the same value:  $L_{\nu_e} = L_{\bar{\nu}_e} = L$ . The luminosity of  $\nu_{\mu}$  is set to be half that value,  $L_{\nu_{\mu}} = 0.5 \times L$ , as in Ohnishi et al. (2007). The numerical code for hydrodynamics is based on the central scheme, which is a popular choice at present (see, e.g., Nagakura et al. (2008, 2011)) and the implementation of the light bulb approximation is explained in detail in Nagakura et al. (2013). We employ the multi-nuclei EOS, which gives not only thermodynamical quantities but also the abundance of various light and heavy nuclei up to the mass number  $A \sim 1000$  (Furusawa et al. 2011, 2013).

The heating rates for light nuclei are calculated from the analytic formula given in Haxton (1988).

$$Q_i = \frac{\rho X_i}{m_u} \frac{31.6 \text{ MeV s}^{-1}}{(r/10^7 \text{ cm})^2} \left[ \begin{aligned} & \frac{L_{\nu_e}}{10^{52} \text{ ergs s}^{-1}} \left( \frac{5 \text{ MeV}}{T_{\nu_e}} \right) \frac{A_i^{-1} \langle \sigma_{\nu_e}^+ E_{\nu_e} + \sigma_{\nu_e}^0 E_{\text{NC}}^i \rangle_{T_{\nu_e}}}{10^{-40} \text{ cm}^2 \text{ MeV}} \\ & + \frac{L_{\bar{\nu}_e}}{10^{52} \text{ ergs s}^{-1}} \left( \frac{5 \text{ MeV}}{T_{\bar{\nu}_e}} \right) \frac{A_i^{-1} \langle \sigma_{\bar{\nu}_e}^- E_{\nu_e} + \sigma_{\bar{\nu}_e}^0 E_{\text{NC}}^i \rangle_{T_{\bar{\nu}_e}}}{10^{-40} \text{ cm}^2 \text{ MeV}} \\ & + \frac{L_{\nu_{\mu}}}{10^{52} \text{ ergs s}^{-1}} \left( \frac{10 \text{ MeV}}{T_{\nu_{\mu}}} \right) \frac{A_i^{-1} \langle \sigma_{\nu_{\mu}}^0 E_{\text{NC}}^i + \sigma_{\bar{\nu}_{\mu}}^0 E_{\text{NC}}^i \rangle_{T_{\nu_{\mu}}}}{10^{-40} \text{ cm}^2 \text{ MeV}} \end{aligned} \right], \quad (5)$$

where  $i$  specifies a light nucleus,  $d, t, h$  or  $\alpha$ ;  $A_i$  and  $X_i$  are the mass number and mass fraction of nucleus  $i$ , respectively;  $m_u$  is the atomic mass unit; the average over the neutrino spectrum is denoted as  $\langle \rangle_T$ . The energy-transfer coefficients for deuterons are calculated from Table I in Nakamura et al. (2009) for both the neutral-current (NC),  $\langle \sigma_{\nu}^0 E_{\text{NC}}^i \rangle_T$ , and the charged-current (CC),  $\langle \sigma_{\nu}^{\pm} E_{\nu} \rangle_T$ . The energy-transfer coefficients for the nuclei with  $A_i = 3$  (tritons and helions) are obtained from Table II in O'Connor et al. (2007) for NC. As for the CC interactions between tritons and  $\bar{\nu}_e$ , we utilize Table I in Arcones et al. (2008). The other CC reactions involving tritons or helions are not included in our simulations, since neither the energy-transfer coefficients nor the cross sections are available. The effects of helions are negligible, however, since the abundance of helions is much smaller than nucleons and dominant light nuclei ( $d$  and  $\alpha$ ). The energy-transfer coefficients for alpha particles are derived from Table II in Haxton (1988) for CC whereas we utilize

for NC the fitting formula provided by Haxton (1988),

$$A_i^{-1} \langle \sigma_\nu^0 E_{\text{NC}}^i + \sigma_\nu^0 E_{\text{NC}}^i \rangle_{T_\nu} = \alpha \left[ \frac{T_\nu - T_0}{10 \text{MeV}} \right]^\beta, \quad (6)$$

where the parameters are chosen to be  $\alpha = 1.28 \times 10^{-40} \text{ MeV cm}^2$ ,  $\beta = 4.46$  and  $T_0 = 2.05 \text{ MeV}$  following Gazit et al. (2004). The cooling reactions involving light nuclei are ignored, since the reaction rates are not available at the moment. In this sense, the influences of light nuclei that we find in this paper should be regarded as the maximum. We also ignore the contributions of charged-current interactions of light nuclei to the evolution of electron fraction Eq. (4) as in Ohnishi et al. (2007), since they are quite minor compared to the contributions of nucleons in most regions as demonstrated at the end of the next section.

As the first step of the simulations, we prepare the initial conditions, which are spherically symmetric, steady accretion flows that are stable to radial perturbations (Yamasaki et al. 2005; Ohnishi et al. 2006; Nagakura et al. 2013). The inelastic interactions of neutrinos with light nuclei,  $Q_{d,t,h,\alpha}$ , are also included in these computations. We start dynamical simulations, adding radial-velocity perturbations of 1 %, which are proportional to  $\cos\theta$ . We vary the luminosity  $L$  and mass accretion rate  $\dot{M}$  and investigate the influences of light nuclei on dynamics under different physical conditions. We refer to the normalized neutrino luminosity  $L_{52} \equiv L/(10^{52} \text{erg/sec})$  and mass accretion rate  $\dot{M}_{sun} \equiv -\dot{M}/(M_\odot \text{s}^{-1})$  in specifying models.

### 3. Result

In the following subsections we first discuss the influences of light nuclei on the initial states, that is, the spherically symmetric, steady accretion flows through the standing shock wave onto the proto-neutron star. Then, a 1D simulation is presented to give an insight into the roles of light nuclei. Finally, we describe the results of 2D dynamical simulations in detail.

In Table 1, we compare the heating rates per baryon for light nuclei, which can be evaluated without referring to matter profiles. We set  $r = 100 \text{ km}$ ,  $L_{52} = 5.0$  and  $X_i = 1.0$ . Note that the cooling rates are not subtracted here for comparison. We set  $X_p = X_n = 0.5$  in the evaluations of the heating rates for nucleons. It is found that deuterons have the heating rates per baryon that are comparable to those of nucleons. Tritons, helions and alpha particles have rather small heating rates per baryon. Muon neutrinos do not heat nucleons but light nuclei thorough NC, since the former has no internal degree of freedom that can be excited.

#### 3.1. Steady state

The left panel of Fig. 1 displays the shock radii  $r_s$  in the spherically symmetric, steady accretion flows with and without the heating of light nuclei for  $L_{52} = 5.2$  and 6.2. We can see the shock radii

are not significantly affected by this change. Higher luminosities and lower mass accretion rates make the light nuclei a little bit more influential on the structures of the steady states. Note also that higher luminosities and lower mass accretion rates result in the steady states that are closer to the critical ones and small variations may have a greater effect. The center and right panels of Fig. 1 show the variations of shock radii, which are defined as  $(r_s - r_{s0})/r_{s0} \times 100$  [%] with the shock radius  $r_{s0}$  for no light-nuclei heating, for the three cases, in which we include either the heating of all light nuclei or that of only deuterons or alpha particles, respectively. The results indicate that deuterons are always one of the main contributors to the heating though the resultant variations are not so large. On the other hand, alpha particles can push the shock wave only when the mass accretion rate is small. The nuclei with  $A_i = 3$  have little influence in any condition, since tritons and helions are much less abundant than the other two light nuclei.

Figure 2 displays the profiles of the mass fraction and heating rate of each nuclear species for two models, which include heating by all light nuclei. For the model with  $L_{52} = 5.2$  and  $\dot{M}_{sun} = 1.5$ , the shock radius is  $\sim 140$  km and the deuteron-heating is second dominant after that of nucleons in the gain region, that is, the region between the gain radius  $r_g$  and shock radius  $r_s$ . The gain radius  $r_g$  is defined as the radius, at which the neutrino heating is equal to the neutrino cooling and there is no net energy gain. For the model with  $L_{52} = 6.2$  and  $\dot{M}_{sun} = 0.5$ , alpha particles contribute to the heating as well as nucleons in the outer part of the gain region. This difference between deuterons and alpha particles can be also seen in Fig. 3, which indicates in the  $\rho$ - $T$  plane under the condition of  $Y_e = 0.5$  the regions, where deuterons and alpha particles are abundant. Superimposed are the actual  $(\rho, T)$  values obtained in the gain region. Note that the electron fractions obtained in the simulations take various values between 0.3 and 0.5 in the gain region. However, the deuteron-rich and alpha-rich regions for  $Y_e = 0.3$  are not much different from those for  $Y_e = 0.5$ .

For the model with  $L_{52} = 6.2$  and  $\dot{M}_{sun} = 0.5$  (brown), the shock radius is rather large and the plots of  $(\rho, T)$  pairs obtained in this model extend to lower densities and temperatures, which favor the existence of alpha particles. For the model with  $L_{52} = 5.2$  and  $\dot{M}_{sun} = 1.5$  (magenta), on the other hand, all the  $(\rho, T)$  pairs are outside the region, in which the fraction of alpha particles is larger than 10 %, and are located close to the region, in which more than 1 % of deuteron fractions is realized. Note that deuterons have the energy-transfer coefficients more than 10 times larger than those of alpha particles as shown in Tab. 1. Deuterons can hence make some small contributions to the total heating rates even if the fraction is as small as  $\sim 1$  %. Deuterons and alpha particles can contribute to the neutrino heating at the inner and outer parts of the gain region, respectively. As a result, the larger shock radius leads to the more efficient heating by alpha particles than by deuterons.

So far we have investigated the differences that the heating via light nuclei may make by arbitrarily switching them on and off for the same background models. It may be interesting, however, to make comparisons against the models, in which not only the heating but also the existence of the light nuclei other than alpha particles is entirely neglected. There are two reasons for this: first, the EOS's that have been commonly employed in supernova simulations thus far

consider only alpha particles as light nuclei; second, if light nuclei did not exist in the first place, nucleons would be more populous, taking their places, and could be efficiently heated, thus reducing or even nullifying the differences we have observed above.

In order to see this, we employ the Shen’s EOS (Shen et al. (2011)), one of the standard EOS’s for supernova simulations, in which only alpha particles are included as light nuclei, and construct spherically symmetric, steady accretion flows and investigate the differences that  $d, t$  and  $h$  make. Strictly speaking, there are some differences between our and Shen’s EOS other than the treatment of light nuclei. For example, the Shen’s EOS takes into account a single representative heavy nuclei whereas our EOS handles the ensemble of them. This is not so important in the post-shock region of our concern, however, since the nucleons and light nuclei are dominant there. Even the treatment of alpha particles is different between the two EOS’s, since we take into account the ambient matter effects in evaluating the mass of alpha particles (Furusawa et al. 2013). This difference, however, manifests itself only at high densities  $\rho \gg 10^{11} \text{g/cm}^3$ , the density at the inner boundary in our models.

Figure 2 shows that the abundances of nucleons and alpha particles are almost identical between the corresponding models. As a result, the heating via nucleons does not differ significantly although both the mass fractions and heating rates of nucleons and alpha particles are slightly larger in the model with the Shen’s EOS. For instance, the mass fractions of nucleons and alpha particles in the model with our EOS are smaller by 0.9 % and 0.3 %, respectively, than those in the model with the Shen’s EOS at  $r = 130 \text{ km}$  for  $L_{52} = 5.2$  and  $\dot{M}_{sun} = 1.5$  due to the existence of light nuclei other than alpha particles. And the heating rates per baryon ( $Q_E, Q_\alpha$ ) are (237.0, 0.3643) in MeV/sec with our EOS, which should be compared with the values (238.6, 0.3653) that are obtained with the Shen’s EOS. The total heating rate,  $Q_E + Q_d + Q_t + Q_h + Q_\alpha$ , in the model with our EOS, however, is larger than the sum of  $Q_E$  and  $Q_\alpha$  in the model with the Shen’s EOS because of the contribution from deuterons,  $Q_d = 3.264$ . As a result, the shock radius in the former model is slightly larger than that in the latter model. The difference is clearer in the case of  $L_{52} = 6.2$  and  $\dot{M}_{sun} = 0.5$ . To be fair, we point out that the  $Q_E$  includes cooling but others do not completely (see section 2). If we compare the absorptions of neutrinos alone, the total rates are larger in the models with the Shen’s EOS, since the contribution from nucleons overwhelms that from deuterons. Comparisons in dynamical contexts will be given later.

### 3.2. 1D simulation

To obtain the basic features of the heating by light nuclei in the dynamical settings, we perform a spherically symmetric 1D simulation. We employ 300 radial mesh points as explained in section 2. Figure 4 shows the entropy evolution for the model with  $L_{52} = 5.4$  and  $\dot{M}_{sun} = 1.0$ . Although we do not add any perturbation initially, numerical noises induce small radial oscillations that grow gradually. It can be seen that matter just below the shock wave has low entropy when the shock radius is large. It should be also noted that the entropy for the same shock radius is smaller

when the shock is receding than it is proceeding. This asymmetric feature becomes clearer as the shock radius gets larger. In Fig. 5, we compare the time evolutions of the integrated heating rate of each nuclear species along with the shock and gain radii. The shock radius is defined as the iso-entropic surface of  $s = 5.0 k_B$ , where  $k_B$  is the Boltzmann constant. The heating rates are integrated over the gain region as  $\int_{\text{gain}} Q_i d\mathbf{r}^3$  and given in the unit of  $10^{52} \text{ erg s}^{-1}$ . We can see that the heating rate of alpha particles changes roughly in step with the shock radius, since the larger shock radius leads to the greater fractions of alpha particles. The peak time in the heating rate of alpha particles delays from the time of the local maximum in the shock radius because of the asymmetric feature in the entropy mentioned above. It is also found that the heating of alpha particles is more important than that of deuterons after the shock wave revives and goes outward ( $t > 400 \text{ ms}$ ). On the other hand, the heating rates of deuterons reach a local maximum when the gain and shock radii are small, since matter has high densities and favors deuterons. Furthermore, since deuterons are located closer to the neutrino sphere, they attain the heating rates as high as 1–10 % of those of nucleons. These results indicate that alpha particles and deuterons heat matter in different phases in the oscillation of the shock wave. Although tritons and helions are similar to deuterons, they are quite minor.

### 3.3. 2D simulations

Figure 6 displays the time evolutions of average shock radii for four models, in which all light nuclei, only deuterons, only alpha particles and no light nuclei are taken into account in the heating sources, respectively. The results of the model, in which we employ the Shen’s EOS and take into account the heating via alpha particles, are also shown and discussed later. The models without deuteron-heating do not succeed in the shock revival for  $L_{52} = 5.1$ , whereas the other two models do though it takes longer times. For  $L_{52} = 5.2$ , on the other hand, all models produce shock revival. We can see that the heating by deuterons and alpha particles both reduce the time to shock revival. The same trend is also seen in the models with  $L_{52} = 6.3$  and  $\dot{M}_{sun} = 1.5$ . These results suggest that the heating of light nuclei, especially deuterons, is helpful for shock revival. Note, however, that this may be too naive, since the time to shock revival is known to be sensitive to various ingredients such as the initial perturbations when the neutrino luminosity is close to the critical value. In fact, the models with  $L_{52} = 6.0$  and  $\dot{M}_{sun} = 1.5$  show the opposite trend when we include the deuteron-heating: the models without the deuteron-heating can gain larger energies through the heating via nucleons alone than other models. This is because the deuteron-heating prevents the shock wave from shrinking in the first place and reduces the heating via nucleons, since matter tends to be farther away from the neutrino sphere. For instance, at the time  $t = 210 \text{ ms}$ , when all the models with  $L_{52} = 6.0$  and  $\dot{M}_{sun} = 1.5$  hit the local minimum in the average shock radius, the values of the average shock radius and the angle-averaged heating rate per baryon for nucleons are 178 km and 223 MeV/sec, respectively, in the model without light-nuclei heating, whereas they are 183 km and 211 MeV/sec in the model with only deuteron-heating. Although we cannot find a clear trend when it is helpful for shock revival, the deuteron-heating is non-negligible regardless. Alpha

particles do not work that way, on the other hand. They heat matter when the shock wave has large radii as discussed in section 3.2 and, as a result, do not affect the shock recession. The model with the alpha-particle-heating alone has almost the same shock radius 177 km at  $t = 210$  ms. The heating via alpha particles is hence always favorable for shock revival whenever it is effective.

Comparisons between the models with our and Shen’s EOS’s are a bit more difficult due to the inherent intricacies of shock revival mentioned above. We can recognize some trends in Fig. 6, however. As noted in section 3.1, the heating via nucleons alone is larger in the models with the Shen’s EOS whereas the total heating rates are greater for the models with our EOS thanks to the contribution from deuterons. In accordance with this, shock revival occurs earlier in the models that employ our EOS and incorporate the heating via deuterons than in the corresponding models with the Shen’s EOS. The order is reversed in some cases if the heating of deuterons is switched off in the models with our EOS. For example, the stalled shock is revived at  $t \sim 800$  ms for the Shen’s EOS in the case of  $L_{52} = 5.1$ ; for our EOS, it happens at  $t \sim 600$  ms if the heating of deuterons is included whereas the shock remains stalled even at  $t \sim 1000$  ms if it is turned off. In the same way, the model with the Shen’s EOS for  $L_{52} = 6.0$  shows the intermediate time-evolution between the models that employ our EOS with and without the deuteron-heating. It should be reminded, however, that other differences such as the preheating of nucleons ahead of the shock wave may have some influences on the results.

We now focus on the model with  $L_{52} = 5.2$  and  $\dot{M}_{sun} = 1.0$  that includes the heating by all light nuclei to explore in more detail the role of light nuclei in the evolution of the shock wave. The shock oscillation grows linearly by  $t \sim 150$  ms in this model as seen in Fig. 6. The distributions of nucleons and light nuclei are almost spherically symmetric at  $t = 100$  ms as seen in the upper panels of Fig. 7. The heating rates of light nuclei are large in the narrow region near the quasi-steady shock wave at  $t = 100$  ms. At  $t = 200$  and 300 ms, however, we observe the deformed shock waves that have reached the non-linear regime of SASI. In some regions, the light nuclei are abundant indeed and their heating is efficient accordingly. Figure 8 plots the pairs of  $(\rho, T)$  obtained along 5 different radial rays (see Fig. 3). Although they (the black symbols) are initially not located in the regions that are rich in light nuclei, the turbulence in the non-linear SASI broadens the distributions. Figure 9 shows the mass fractions and the heating rates of different nuclear species along the radial ray with  $\theta = 180^\circ$  at  $t = 200$  ms and another one with  $\theta = 0^\circ$  at  $t = 300$  ms. The heating rate of deuterons becomes as high as  $\sim 10$  % of that of nucleons at  $t = 200$  ms around the bottom of the gain region. It should be noted that the cooling is subtracted for nucleons in  $Q_E$ , whereas it is not included in  $Q_{d,t,h,\alpha}$  because of the lack of the rates in the literature. There are indeed large cancellations between heating and cooling at the bottom of the gain regions. For instance, the heating and cooling rates per baryon for nucleons are 631 and  $-584$  MeV/sec per baryon at  $r = 110$  km along the radial ray with  $\theta = 180^\circ$  at  $t = 200$  ms. If we compare the pure heating rates, deuterons have 4.73 MeV/sec per baryon, which is just 0.75 % of the pure heating rate for nucleons in the same example. Around the same time the shock wave moves northwards ( $\theta = 0^\circ$ ) and the matter in the southern part ( $\theta = 180^\circ$ ) goes down deep into the central region.

The orange symbols in the top panel of Fig. 8 indicate that the matter in this southern part has low entropies, resulting in more deuterons near the bottom of the gain region than the matter in other parts. At  $t = 300$  ms, the shock wave reaches at  $\sim 400$  km and the heating of alpha particles is dominant for the same reasons we have explained in Fig. 2. We can see in the bottom panel of Fig. 8 that the matter along the radial ray with  $\theta = 0^\circ$  has also lower entropies and as a consequence deuterons and alpha particles are abundant in the regions of high and low densities, respectively. Both at  $t = 200$  and 300 ms, deuterons have the heating rates comparable to those of nucleons near the bottom of the gain regions. The heating rates of alpha particles are  $\sim 10$  % of those of nucleons around the shock wave.

Figure 10 displays the time evolutions of the integrated heating rate of each nuclear species together with the shock and gain radii along the two radial rays with  $\theta = 0^\circ$  and  $90^\circ$ . The integrated heating rate for the specific direction is calculated as  $4\pi \int_{r_g(\theta)}^{r_s(\theta)} Q_i(r, \theta) r^2 dr$  in the same way as for the 1D model in Fig. 5. The heating rates of deuterons and alpha particles are about 1 % and 0.1 %, respectively, of those of nucleons in the linear phase of SASI. However, both of them are much more efficient in the subsequent non-linear evolutions of SASI and shock revival. We can see that deuterons and alpha particles have different temporal variations in the heating rates, which is ascribed to the fact that they occupy different parts of the gain region as explained in section 3.2. Note that the heating of light nuclei occurs quite inhomogeneously and the local heating can be more efficient than the average as shown in Fig. 9.

In the models explored so far, the temperature of  $\nu_\mu$  is assumed to be 10 MeV. However, this value may be too high. In fact, recent simulations tend to predict the  $\nu_\mu$  temperatures much closer to those of  $\nu_e$  and  $\bar{\nu}_e$  (e.g. Janka (2012)). We hence repeat some simulations with  $T_{\nu_\mu} = 5$  MeV. As shown in Tab. 1, the  $\nu_\mu$ -heating rate per baryon is reduced by a factor of 10. The decrease in the net heating rates is particularly severe for tritons, helions and alpha particles, since NC interactions with  $\nu_\mu$  are dominant for the heating of these species. On the other hand, the total heating rates of deuterons are reduced by only 24 % because CC interactions with  $\nu_e$  and  $\bar{\nu}_e$  are more important. Figure 11 shows the temporal evolutions of the average shock radii for the models with  $L_{52} = 5.2$  and  $\dot{M}_{sun} = 1.0$ , the counter parts of those presented in Fig. 6. The results are qualitatively different. In fact, shock revival occurs earlier without the heating of deuterons although the shock radius is larger at  $t \sim 200$  ms with the deuteron-heating. This occurs because the heating of nucleons is reduced in the presence of deuterons during the shock expansion at  $t \sim 200$  ms, which is similar to what we observed in the models for  $T_{\nu_\mu} = 10$  MeV with  $L_{52} = 6.0$  presented in Fig. 6. The difference between the models with and without alpha particles is smaller for  $T_{\nu_\mu} = 5$  MeV than for  $T_{\nu_\mu} = 10$  MeV. Figure 12, the counter part of Fig. 9, displays the mass fractions and heating rates of different light nuclei along the radial ray with  $\theta = 180^\circ$  at  $t = 200$  ms. Although the dynamics is stochastic owing to the turbulence induced by SASI and the shock positions are different between the models with  $T_{\nu_\mu} = 5$  MeV and 10 MeV, the heating by deuterons are not so significantly decreased thanks to the CC contributions, whereas the heating rates of alpha particles are diminished by a factor of 10. Provided the high energy-dependence of the  $\nu_\mu$ -heating, we think

that our standard models with  $T_{\nu_\mu} = 10$  MeV give the upper limit of the  $\nu_\mu$ -heating whereas the models with  $T_{\nu_\mu} = 5$  MeV will set the lower limit.

In our standard models, the CC interactions on light nuclei are ignored in the temporal evolution of electron fraction. One may be worried, however, that this could affect the dynamics, since the CC interactions are dominant in the heating of deuterons. Note that the CC contributions are much smaller for  $t, h$  and  $\alpha$ . In order to address this issue, we have included the contributions of deuterons and tritons in Eq. (4), the former of which is given by

$$Q_{Nd} = X_d \frac{31.6 \text{ s}^{-1}}{(r/10^7 \text{ cm})^2} \left[ \frac{L_{\nu_e}}{10^{52} \text{ ergs s}^{-1}} \left( \frac{5 \text{ MeV}}{T_{\nu_e}} \right) \frac{A_d^{-1} \langle \sigma_{\nu_e}^+ \rangle_{T_{\nu_e}}}{10^{-40} \text{ cm}^2} - \frac{L_{\bar{\nu}_e}}{10^{52} \text{ ergs s}^{-1}} \left( \frac{5 \text{ MeV}}{T_{\bar{\nu}_e}} \right) \frac{A_d^{-1} \langle \sigma_{\bar{\nu}_e}^- \rangle_{T_{\bar{\nu}_e}}}{10^{-40} \text{ cm}^2} \right]. \quad (7)$$

This expression is obtained by just replacing the energy-transfer coefficient  $\langle \sigma_{\nu}^{\pm} E_{\nu} \rangle_{T_{\nu}}$ , with the cross section averaged over the neutrino spectrum  $\langle \sigma_{\nu}^{\pm} \rangle_{T_{\nu}}$ , in Eq. (5). We ignore the other contributions. For tritons, only the electron-type anti-neutrinos are included, since the cross section for  $\nu_e$  is currently unavailable. Note, however, that the contribution of tritons is negligible anyway as shown shortly.

We initially construct the spherically symmetric, steady accretion flows and then perform 2D simulations with  $Q_{Nd}$  and  $Q_{Nt}$  being incorporated. The neutrino luminosity and mass accretion rate are fixed to  $L_{52} = 5.2$  and  $\dot{M}_{sun} = 1.0$  here. It turns out that the temporal evolution of the shock wave is unchanged from that presented in Fig. 6, which justifies the neglect of these effects in the standard models. In fact, Fig. 13 demonstrates by comparing  $Q_{Nd}$  and  $Q_{Nt}$  with  $Q_N$ , the contribution of nucleons, at  $t = 0, 200$  ms that  $Q_{Nd}$  is about 0.1 % of  $Q_N$  in most regions and  $Q_{Nt}$  is always negligibly small. Although we can see in the initial condition a slight increase in  $Y_e$  by the inclusion of  $Q_{Nd}$  and  $Q_{Nt}$ , the difference disappears by  $t = 200$  ms.

The reasons why deuterons are non-negligible heating sources, giving 1-10 % of the nucleon contributions, but they do not contribute to the evolution of  $Y_e$  are the following: (1) the net heating rate of nucleons,  $Q_E$ , is an outcome of rather big cancellations between heating and cooling near the gain radius whereas such cancellations are not so large in  $Q_N$ ; as a result  $Q_N$  is much greater than  $Q_{Nd}$  in the region where the deuteron-heating is efficient; (2) the  $Y_e$  evolution is controlled by the competition between the electron-type neutrinos and anti-neutrinos; according to the current formula,  $Q_{Nd}$  is given as  $Q_{Nd} = Q_{Nd}(\nu_e d) - Q_{Nd}(\bar{\nu}_e d) = 0.188 Q_{Nd}(\nu_e d)$  and the cancellation is much larger than for  $Q_N$ ; (3) the NC reactions contribute 12 and 33 % to  $Q_d$  for  $T_{\nu_\mu} = 5$  and 10 MeV, respectively, but none to  $Q_{Nd}$ .

To summarize, the heating via light nuclei is non-negligible in the non-linear phase of SASI, in which various values of  $(\rho, T)$  are realized, whereas they are minor in the linear stage. Among light nuclei, deuterons play important roles near the bottom of the gain region whereas alpha particles are influential near the shock fronts when the shock wave is expanding and, as a consequence, the

densities and temperatures become lower. The results are rather sensitive to the  $\nu_\mu$  spectrum. If the temperature of  $\nu_\mu$  is as low as that of  $\bar{\nu}_e$ , the heating of alpha particles will be substantially diminished whereas the deuteron-heating is not so much reduced.

#### 4. Summary and Discussions

We have investigated the influences of the inelastic interactions of neutrinos with light nuclei on the dynamics in the post-bounce phase of core-collapse supernovae. We have done 2D numerical simulations of SASI with the assumption of axial symmetry for some representative combinations of the luminosity and mass accretion rate. We have not solved the dynamics of the central part of the core and replaced it with the suitable boundary conditions and have started the simulations from spherically symmetric steady state, adding some perturbations to the radial velocity. The neutrino transport has been handled by the simple light-bulb approximation with the time-independent Fermi-Dirac spectrum. In addition to the ordinary heating and cooling reactions with nucleons, we have taken into account the heating reactions with four light nuclei for the first time. The abundance of light nuclei is provided by the multi-nuclei EOS together with other thermodynamical quantities.

We have found that the evolutions of shock waves in 2D are influenced by the heating of deuterons and alpha particles and that they have different roles. In the initial steady states, the heating by light nuclei is the most efficient for the combination of high neutrino luminosity and low mass accretion rate, since the shock radius is large and the matter near the shock front has the low densities and temperatures that yield a large amount of alpha particles. On the other hand, deuterons are populated near the bottom of the gain region, where matter has higher densities and temperatures. They hence have some impacts on the shock radius regardless of neutrino luminosities and mass accretion rates. From the results of 1D simulations, we have found that the integrated heating rates of deuterons and alpha particles become high at different phases in the oscillations of shock wave: the heating rate of deuterons becomes the highest when the shock radius hits the minimum and the matter compression is the greatest. Whereas the heating via deuterons is constantly effective, the heating of alpha particles becomes important only when the shock wave has large radii and matter has low entropies. The dynamics in 2D is more sensitive to the inclusion of the light-nuclei heating because SASI in the non-linear regime makes the gain region more inhomogeneous and there appear the regions that have densities and temperatures favorable for the existence of light nuclei. The heating rates of light nuclei reach about 10 % of those of nucleons locally. As a consequence, the dynamics of shock revival is influenced by the heating via light nuclei. In particular, the heating by deuterons brings non-negligible changes, which may be positive or negative for shock revival, when the neutrino luminosity is close to the critical value. The results are rather sensitive to the neutrino spectrum. In the case of  $T_{\nu_\mu} = 5$  MeV instead of  $T_{\nu_\mu} = 10$  MeV, the heating of alpha particles is reduced by  $\sim 90$  % whereas the heating via deuterons are not so much affected, since the CC reactions with  $\nu_e$  and  $\bar{\nu}_e$  are more important for the deuteron-heating.

The numerical simulations in this paper are admittedly of experimental nature and the numbers we have obtained may be subject to change in more realistic simulations. We need more systematic investigations, varying not only the neutrino luminosity and mass accretion rate but also the neutrino temperature, mass of a central object and initial perturbation. The cooling reactions of light nuclei such as  $d + e^- \rightarrow n + n + \nu_e$  and  $n + p \rightarrow d + \nu + \bar{\nu}$  should be incorporated in the calculations, since deuterons are abundant in the cooling regions as shown in Figs. 2 and 9. Recently, Nasu et al. (2013) demonstrated that the existence of deuteron reduces the neutrino emissions by the electron- and positron captures, since the capture rate of deuterons is lower than that of nucleons. They made a comparison of the total  $e^\pm$ -capture rates between the models with and without deuterons at 150 ms after core bounce, employing the compositions of light nuclei calculated in Sumiyoshi et al. (2008). Figs. 1 and 2 in Nasu et al. (2013) indicate that this effect becomes remarkable inside the neutrino sphere but the reduction factor goes down below a few percent near the gain radius ( $r \sim 90$  km). Note that this effect is included in our models except for the  $e^\pm$ -captures on deuterons. Although the latter rates are not available for us at present, their contributions to the cooling would be less than a few percent of the cooling rates of nucleons in the gain region and the discussion in this article would not be changed significantly. Of course the reactions will become important at the bottom of the cooling region. The neutrino transport should be improved so that the neutrino emission from accreting matter could be properly treated. For more realistic simulations the central part of the core should be also solved self-consistently. Last but not least the difference between 2D and 3D should be made clear. These issues are currently being tackled and will be reported elsewhere.

S. F. thanks T. Sato, S. Nasu, T. Fischer, W. I. Nakano and Y. Yamamoto for their useful discussions. S. F. is supported by the Japan Society for the Promotion of Science Research Fellowship for Young Scientists. This work is partially supported by the Grant-in-Aid for Scientific Research on Innovative Areas (Nos. 20105004, 20105005), the Grant-in-Aid for the Scientific Research (Nos. 22540296, 24103006, 24244036, 24740165), the HPCI Strategic Program and Excellent Graduate Schools from the Ministry of Education, Culture, Sports, Science and Technology (MEXT) A part of the numerical calculations were carried out on SR16000 at YITP in Kyoto University.

## REFERENCES

- Arcones, A., Martínez-Pinedo, G., O’Connor, E., Schwenk, A., Janka, H.-T., Horowitz, C. J., & Langanke, K. 2008, *Phys. Rev. C*, 78, 015806
- Barnea, N. & Gazit, D. 2008, *Few-Body Systems*, 43, 5
- Blinnikov, S. I., Panov, I. V., Rudzsky, M. A. & Sumiyoshi, K. 2011, *A&A*, 535, A37
- Blondin, J. M., Mezzacappa, A. & DeMarino, C., 2003, *ApJ*, 584, 971

- Botvina, A.S. & Mishustin, I.N. 2004 Phys. Lett. B 584, 233.
- Botvina, A.S. & Mishustin, I.N. 2010 Nucl. Phys. A 843, 98.
- Bruenn, S. W. and Mezzacappa, A. and Hix, W. R. and Lentz, E. J. and Bronson Messer, O. E. and Lingerfelt, E. J. and Blondin, J. M. & Endeve, E. and Marronetti, P. and Yakunin, K. N. 2013, ApJ767, 6
- Buras, R., Rampp, M., Janka, H.-Th. & Kifonidis, K., 2006a, A&A, 447, 1049
- Buras, R., Janka, H.-Th., Rampp, M. & Kifonidis, K., 2006b, A&A, 457, 281
- Burrows, A., Hayes, J. & Fryxell, B. A., 1995, ApJ, 450, 830
- Burrows, A. 2012 arXiv:astro-ph 1210.4921
- Couch, S. M. 2013, ApJ, 765, 29
- Fernández, R. & Thompson, C. 2009a, ApJ, 697, 1827
- Fernández, R. & Thompson, C. 2009b, ApJ, 703, 1464
- Fernández, R. 2010, ApJ, 725, 1563
- Foglizzo, T., Scheck, L. & Janka, H.-Th., 2006, ApJ, 652, 1436
- Foglizzo, T., Galletti, P., Scheck, L., & Janka, H.-T. 2007, ApJ, 654, 1006
- Foglizzo, T., Masset, F., Guilet, J., & Durand, G. 2012, Physical Review Letters, 108, 051103
- Fryer, C. L., Holz, D. E., & Hughes, S. A. 2002, ApJ, 565, 430
- Fryer, C. L. 2004, Astrophys. J. Lett., 601, L175
- Furusawa, S., Yamada, S., Sumiyoshi, K. & Suzuki, H. 2011 ApJ, 738, 178.
- Furusawa, S., Sumiyoshi, K., Yamada S. & Suzuki, H. 2013, arXiv:astro-ph 1305.1508
- Gazit, D. and Barnea, N., 2004 Phys. Rev. C, 70, 8801
- Hanke, F., Marek, A., Mueller, B., & Janka, H.-T. 2012, ApJ755, 138
- Hanke, F. and Marek, A. and Müller, B. and Janka, H.-T. arXiv:astro-ph 1303.6269
- Haxton, W. C. 1988, Physical Review Letters, 60, 1999
- Hempel, M. & Schaffner-Bielich, J. 2010 Nucl. Phys. A 837, 210
- Hempel, M., Fischer, T., Schaffner-Bielich, J. & Liebendörfer, M. 2012, ApJ, 748, 70.

- Herant, M., Benz, W. & Colgate, S., 1992, *ApJ*, 395, 642
- Iwakami, W., Kotake, K., Ohnishi, N., Yamada, S., & Sawada, K. 2008, *ApJ*, 678, 1207
- Iwakami, W., Kotake, K., Ohnishi, N., Yamada, S., & Sawada, K. 2009, *ApJ*, 700, 232
- Janka, H.-T., 2012, *ARNPS*. 62, 407
- Kotake, K., Sato, K., Takahashi, K., 2006, *Reports of Progress in Physics*, 69, 971
- Kuroda, T., Kotake, K., & Takiwaki, T. 2012, *ApJ*, 755, 11
- Lattimer, J. M. & Swesty, F. D. 1991, *Nucl. Phys. A*, 535, 331
- Langanke, K. & Martinez-Pinedo, G., Muüller, B., Janka, H.-Th., Marek, A., Hix, W. R., Juodagalvis, A. & Sampaio J. M. 2008, *Phys. Rev. Lett.*100, 011101
- Marek, A. & Janka, H.-Th., 2009, *ApJ*, 694, 664
- Marek, A., Janka, H.-T., Müller, E. 2009, *A&A*, 496, 475
- Mueller, B., Janka, H.-T., & Heger, A. 2012, *ApJ*, 761, 72
- Murphy, J. W. and Dolence, J. C. & Burrows, A. *ApJ*, 771, 52
- Nagakura, H., & Yamada, S. 2008, *ApJ*, 689, 391
- Nagakura, H., Ito, H., Kiuchi, K., & Yamada, S. 2011, *ApJ*, 731, 80
- Nagakura, H., Yamamoto, Y., & Yamada, S. 2013, *ApJ*, 765, 123
- Nakamura, S. X., Sumiyoshi, K. & Sato, T. 2009, *Phys. Rev. C*80, 035802
- Nakamura, K., Takiwaki, T., Kotake, K., Nishimura, N. *arXiv:astro-ph 1207.5955*
- Nasu, S., Sato, T., Nakamura, S. X., Sumiyoshi, K. Myhrer, F. and Kubodera, K.,2013, *Few-Body Systems*, 54, 1595
- O’Connor, E., Gazit, D., Horowitz, C.J., Schwenk, A., Barnea, N., 2007 *Phys. Rev. C* 75, 055803
- Ohnishi, N., Kotake, K. & Yamada, S. 2006, *ApJ*, 641, 1018
- Ohnishi, N., Kotake, K. & Yamada, S. 2007, *ApJ*, 667, 375
- Ott, C. D. and Abdikamalov, E. and Mösta, P. and Haas, R. and Drasco, S. and O’Connor, E. P. and Reisswig, C. and Meakin, C. A. & Schnetter, E. 2013 *ApJ*, 768, 1150
- Scheck, L., Plewa, T., Janka, H.-T., Kifonidis, K., & Müller, E., 2004, *Phys. Rev. Lett.*, 92, 011103
- Scheck, L., Kifonidis, K., Janka, H., & Müller, E. 2006, *A&A*, 457, 963

- Shen, H., Toki, H., Oyamatsu, K. & Sumiyoshi, K. 1998a, Nucl. Phys. A, 637, 435
- Shen, H., Toki, H., Oyamatsu, K. & Sumiyoshi, K. 1998b, Prog. Theor. Phys., 100, 1013
- Shen, H., Toki, H., Oyamatsu, K. & Sumiyoshi, K. 2011, Astrophys. J. Supplement 197, 20
- Shen G., Horowitz C. J. & Teige S., 2011, Phys. Rev. C, 83, 035802
- Sumiyoshi, K. and Yamada, S. and Suzuki, H. and Shen, H. and Chiba, S. & Toki, H., 2005, ApJ, 629, 922
- Sumiyoshi, K. & Röpke, G. 2008 Phys. Rev. C 77 055804.
- Suwa, Y., Kotake, K., Takiwaki, T., Whitehouse, S. C., Liebendörfer, M. & Sato, K., 2010, PASJ, 62, L49
- Suwa, Y., Kotake, K., Takiwaki, T., Liebendörfer, M., & Sato, K. 2011, ApJ, 738, 165
- Suwa, Y., Takiwaki, T., Kotake, K., Fischer, T. Liebendörfer, M. & Sato, K. 2013, ApJ, 764, 99
- Takiwaki, T., Kotake, K. & Suwa, Y., 2012, ApJ, 749, 98
- Yamasaki, T., & Yamada, S. 2005, ApJ, 623, 1000
- Yamamoto, Y., Fujimoto, S., Nagakura, H., & Yamada, S. 2013 ApJ, 771, 27

Flavor	$n, p$	$d$	$t$	$h$	$\alpha$
$\nu_e$ (CC)	356.8	168.9	0.000	0.000	0.5925
$\bar{\nu}_e$ (CC)	557.5	169.1	8.015	0.000	1.896
$\nu_e$ (NC)	0.000	12.94	0.6656	0.7446	0.008347
$\bar{\nu}_e$ (NC)	0.000	16.83	1.801	1.975	0.4231
$\nu_\mu$ (NC)	0.000	139.0	31.05	32.55	17.61

Table 1: The heating rates of nucleons, deuterons, tritons, helions and alpha particles in unit of MeV/sec per baryon.  $X_p = 0.5$  and  $X_n = 0.5$  are assumed in the calculations for nucleons. The mass fraction of each light nucleus is set to unity in the calculation for light nuclei;  $X_{d,h,t,\alpha} = 1$ . Other parameters are set at  $r = 100$  km,  $L_{\nu_e, \bar{\nu}_e} = 5.0 \times 10^{52}$  erg s $^{-1}$ ,  $L_{\nu_\mu} = 0.5 \times L_{\nu_e, \bar{\nu}_e}$ ,  $T_{\nu_e} = 4$  MeV,  $T_{\bar{\nu}_e} = 5$  MeV and  $T_{\nu_\mu} = 10$  MeV.

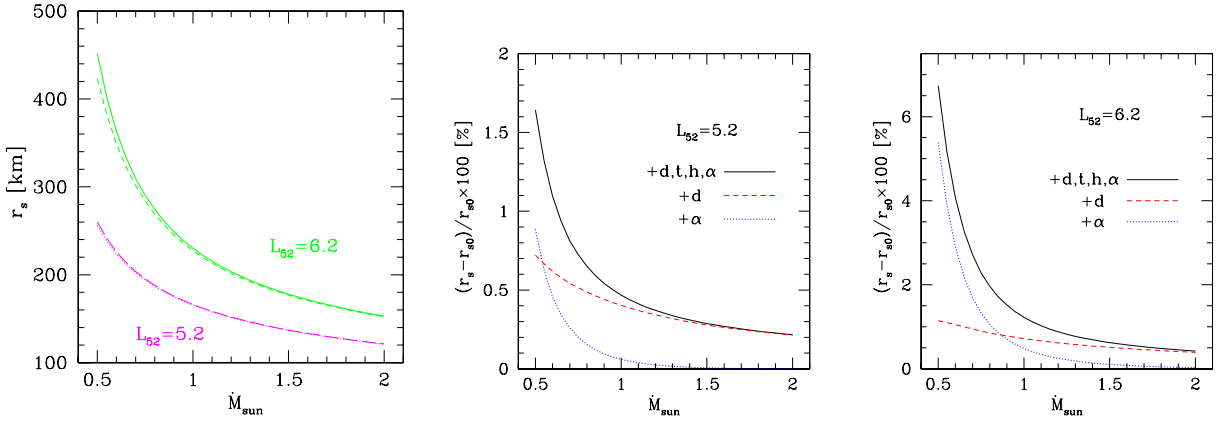


Fig. 1.— The left panel shows the shock radii in the initial steady states for  $L_{52} = 6.2$  with the light-nuclei heating (green solid line) and without it (green dashed line) and for  $L_{52} = 5.2$  with the light-nuclei heating (magenta long dashed line) and without it (magenta dotted line). The center and right panels show the variations of shock radii due to the heating reactions with all light nuclei (black solid line), only deuterons (red dashed line) and only alpha particles (blue dot line).

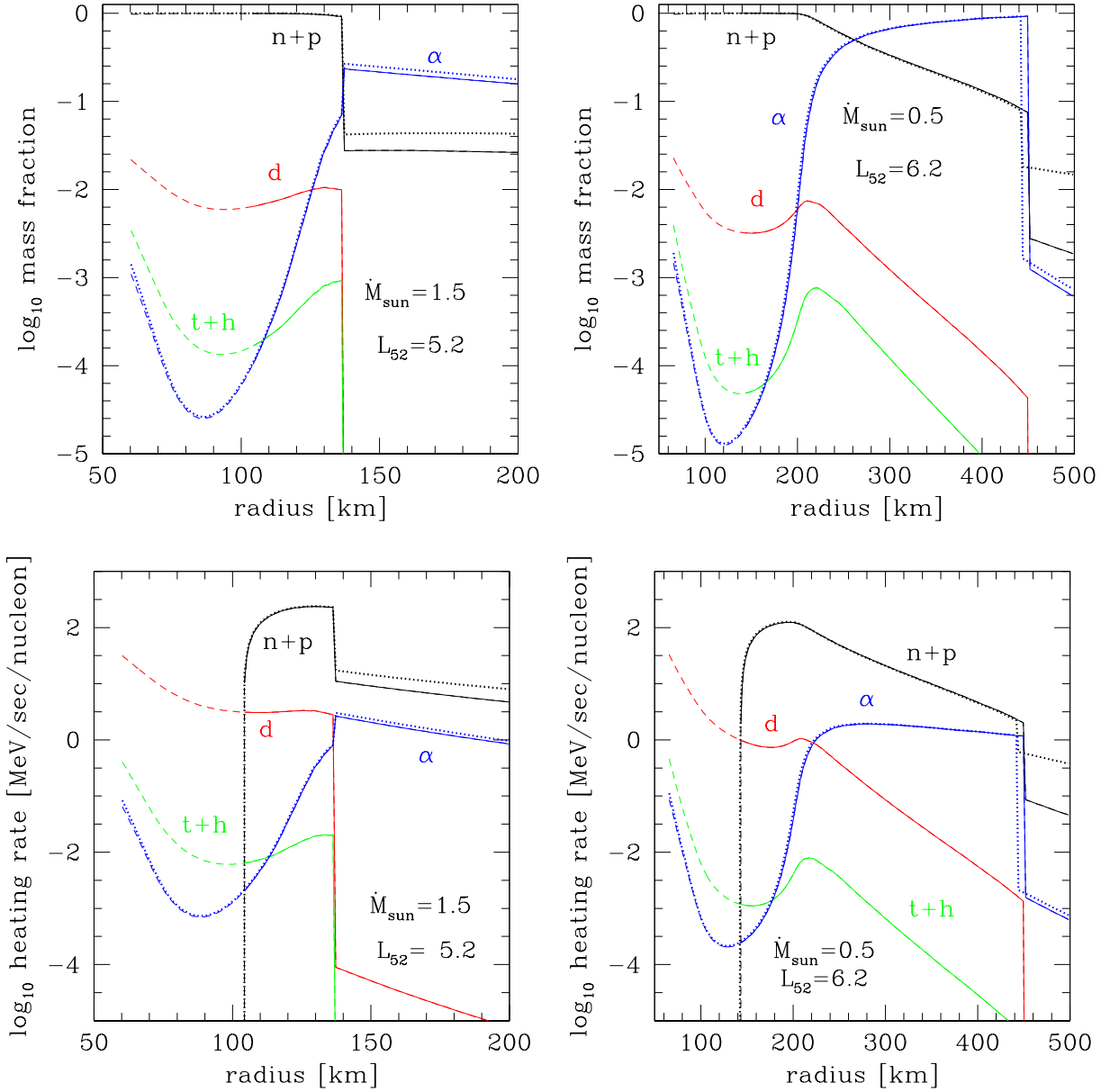


Fig. 2.— The mass fractions (upper) and heating rates per baryon (bottom) of  $A_i = 1$ : protons and neutrons (black),  $A_i = 2$ : deuterons (red),  $A_i = 3$ : tritons and helions (green) and  $A_i = 4$ : alpha particles (blue) for  $L_{52} = 5.2$  with  $\dot{M}_{\text{sun}} = 1.5$  (left panel) and  $L_{52} = 6.2$  with  $\dot{M}_{\text{sun}} = 0.5$  (right panel). Dashed lines indicate the cooling regions where the cooling reaction of nucleons is dominant. Dotted lines are the results of the models with the Shen's EOS for the same  $L_{52}$  and  $\dot{M}_{\text{sun}}$ .

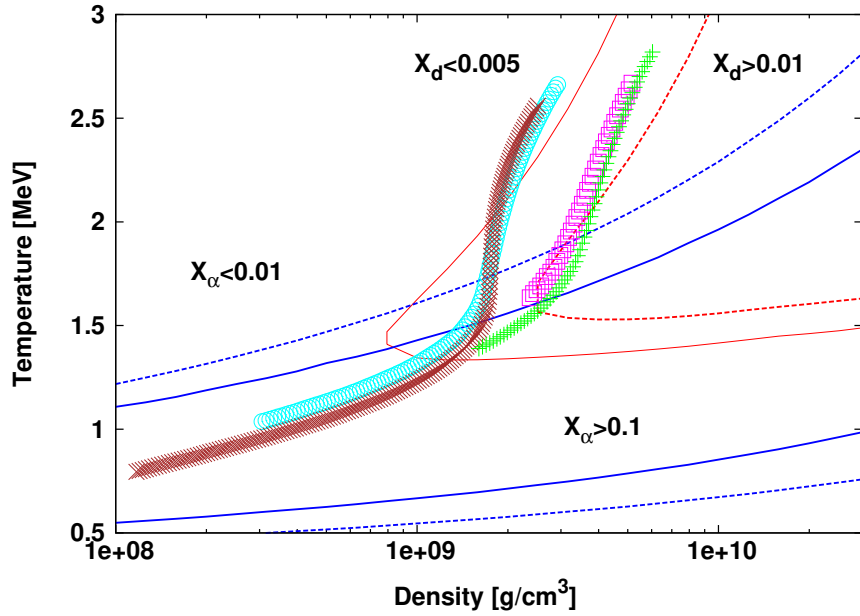


Fig. 3.— The lines show the contours of mass fractions of deuteron  $X_d$  and alpha particle  $X_\alpha$  at  $Y_e = 0.5$  (red thin lines for  $X_d = 0.005$ , red dashed lines for  $X_d = 0.01$ , blue dashed lines for  $X_\alpha = 0.01$  and blue solid lines for  $X_\alpha = 0.1$ ). The symbols mean the densities and temperatures in the gain regions for  $L_{52} = 5.2$  with  $\dot{M}_{sun} = 0.5$  (cyan) and 1.5 (magenta) and  $L_{52} = 6.2$  with  $\dot{M}_{sun} = 0.5$  (brown) and 1.5 (green).

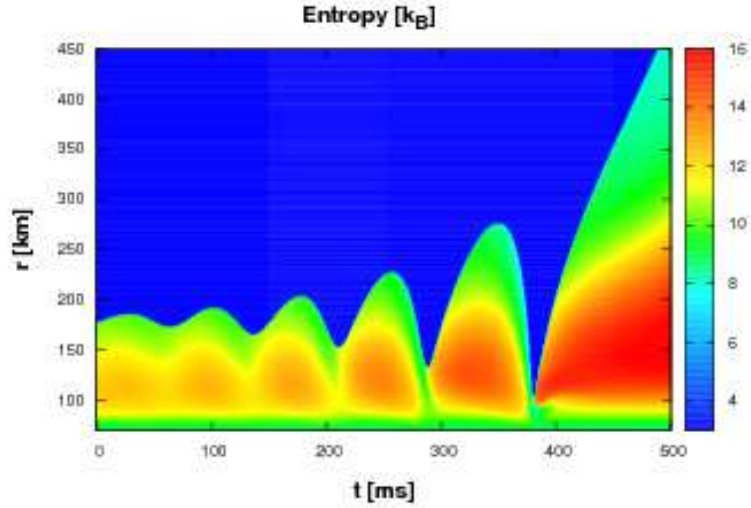


Fig. 4.— The entropy per baryon in the  $(t, r)$  plane for the 1D model with  $L_{52} = 5.4$  and  $\dot{M}_{sun} = 1.0$ .

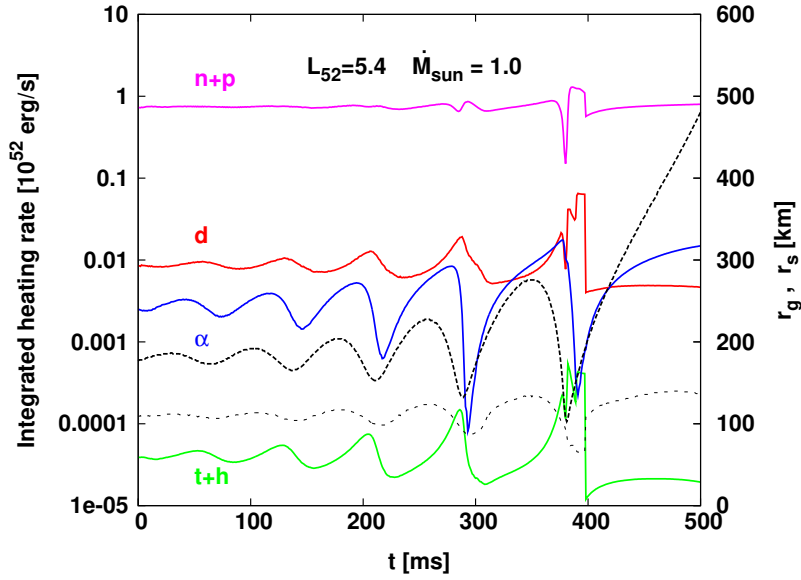


Fig. 5.— The time evolutions of the average shock and gain radii and integrated heating rates of different nuclear species. Black dashed and dotted lines denote the shock and gain radii, respectively. Magenta, red, green and blue lines represent the heating rates of  $A_i = 1$  (nucleons),  $A_i = 2$  (deuterons),  $A_i = 3$  (tritons and helions) and  $A_i = 4$  (alpha particles), respectively.

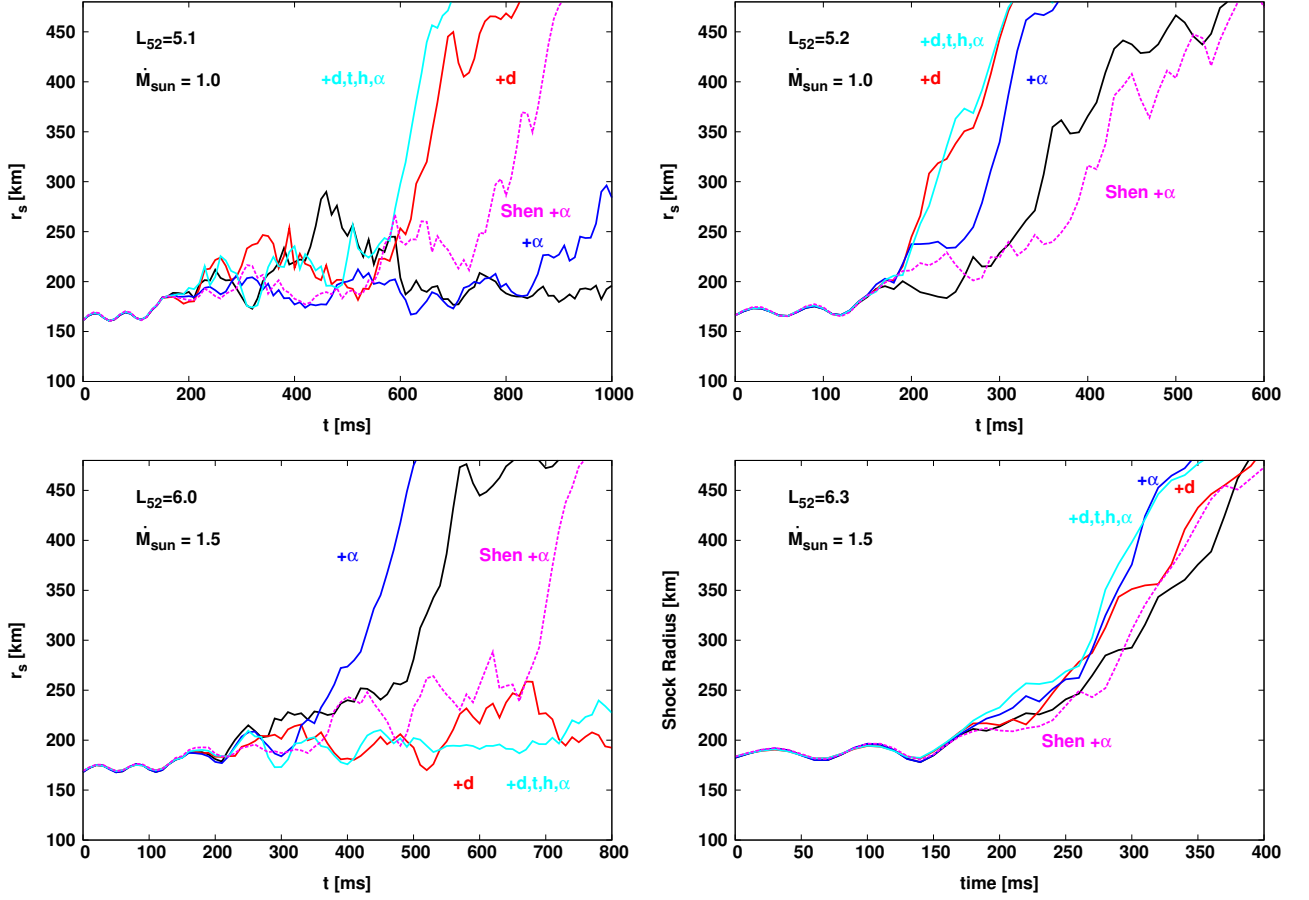


Fig. 6.— The time evolutions of the average shock radii for the models with the heating of all light nuclei (cyan solid lines), only deuterons (red solid lines), only alpha particles (blue solid lines) and no light nuclei (black solid lines) as well as the models with the Shen’s EOS and the heating of alpha particles (magenta dashed lines). The combinations of the luminosity and mass accretion rate are  $L_{52} = 5.1$  and  $5.2$  with  $\dot{M}_{\text{sun}} = 1.0$  and  $L_{52} = 6.0$  and  $6.3$  with  $\dot{M}_{\text{sun}} = 1.5$ .

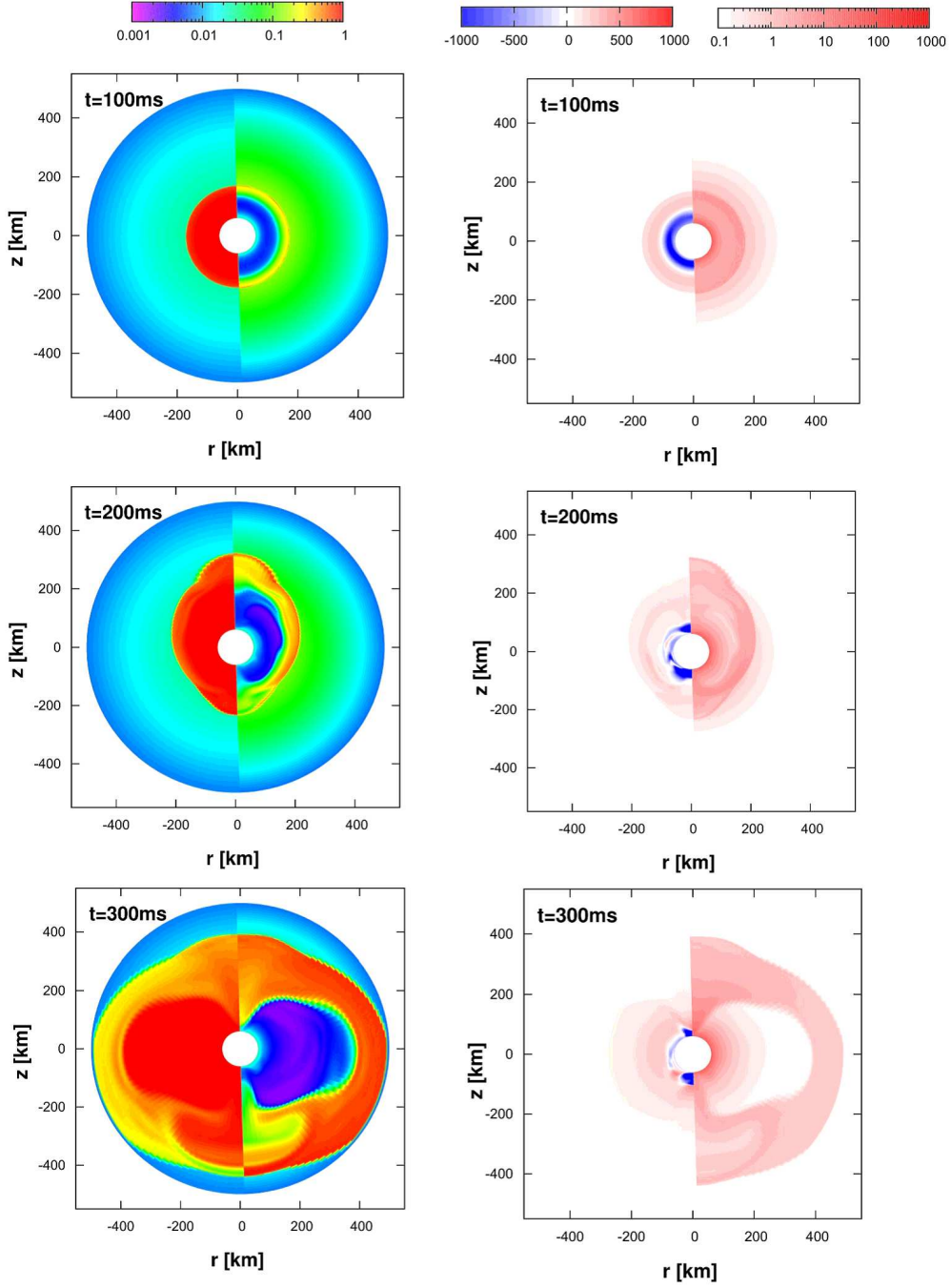


Fig. 7.— The mass fractions of nucleons,  $X_n + X_p$  (left halves of left panels), those of all light nuclei,  $X_d + X_t + X_h + X_\alpha$  (right halves of left panels), the heating and cooling rates per baryon in the unit of MeV/sec of nucleons,  $Q_E \times m_u / \rho$  (left halves of right panels), and those of all light nuclei,  $(Q_d + Q_t + Q_h + Q_\alpha) \times m_u / \rho$  (right halves of right panels). The times are  $t = 100, 200$  and  $300$  ms and the luminosity and accretion rate are  $L_{52} = 5.2$  and  $\dot{M}_{sun} = 1.0$ .

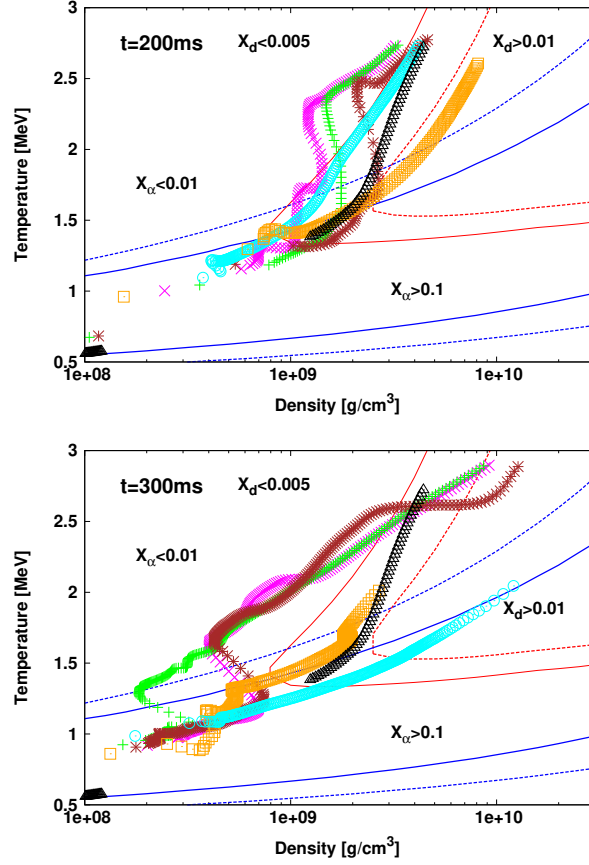


Fig. 8.— The lines are the same as in Fig. 3. The symbols show the densities and temperatures in the gain regions at  $t = 200$  ms (upper panel) and  $300$  ms (lower panel) for the radial rays with  $\theta = 0^\circ$  (cyan),  $45^\circ$  (magenta),  $90^\circ$  (green),  $135^\circ$  (brown) and  $180^\circ$  (orange). The black symbols correspond to the initial spherically symmetric state.

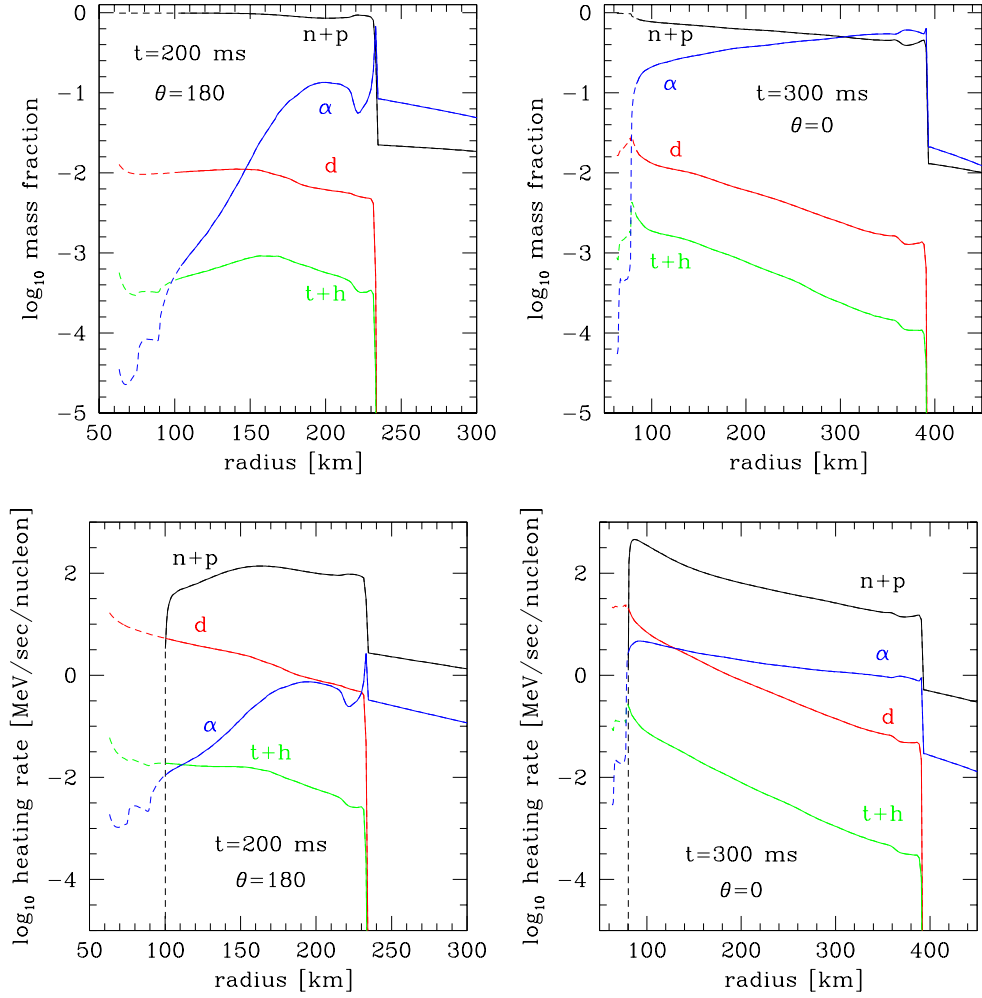


Fig. 9.— The mass fractions (upper panels) and heating rates per baryon (lower panels) along the radial rays with  $\theta = 180^\circ$  at  $t = 200$  ms (left panels) and with  $\theta = 0^\circ$  at  $t = 300$  ms (right panels). The notations of various lines are the same as in Fig. 2.

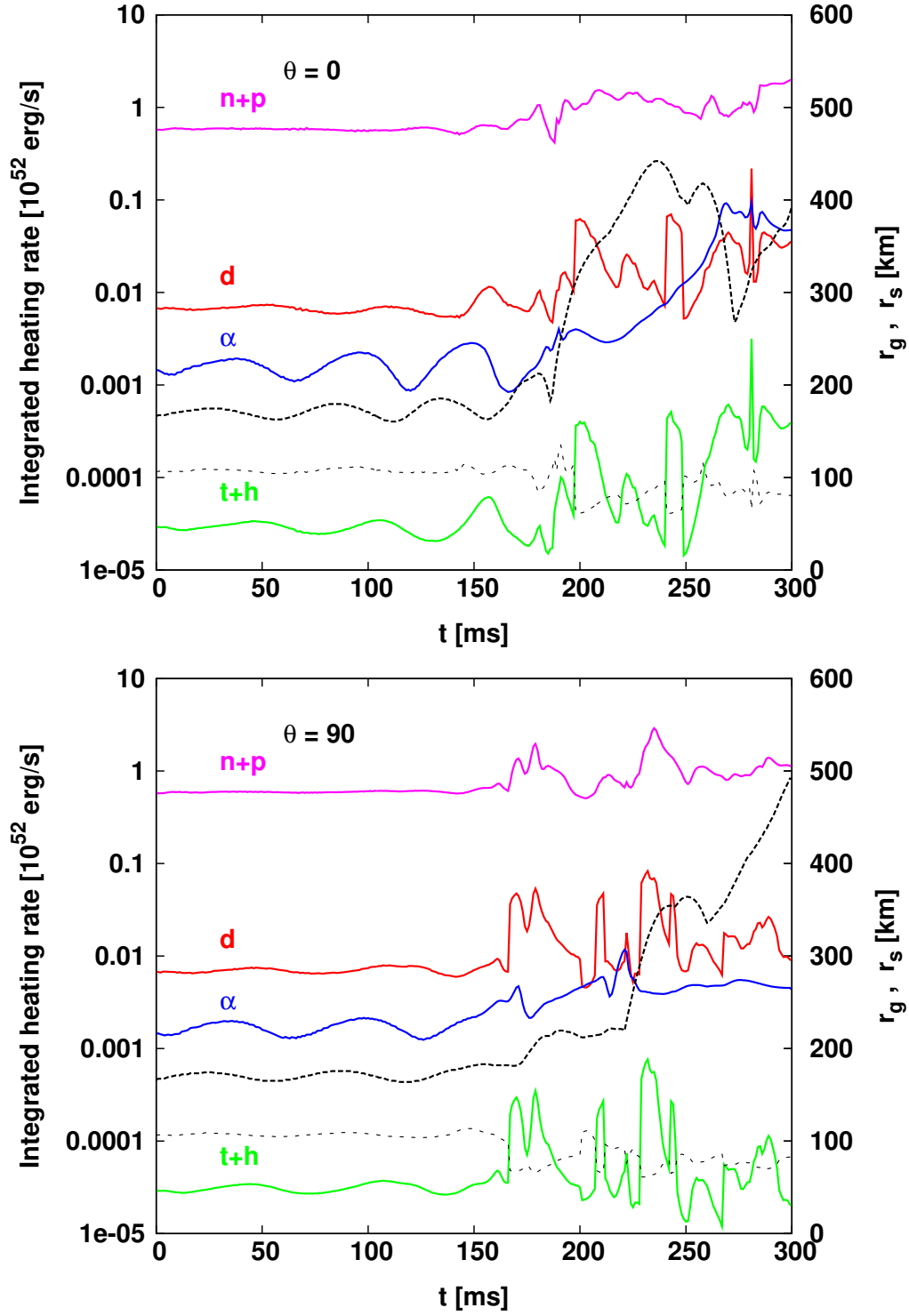


Fig. 10.— The time evolutions of the shock and gain radii and integrated heating rates on the radial rays with  $\theta = 0^\circ$  (upper panel) and  $\theta = 90^\circ$  (lower panel). The notations of various lines are the same as in Fig. 5.

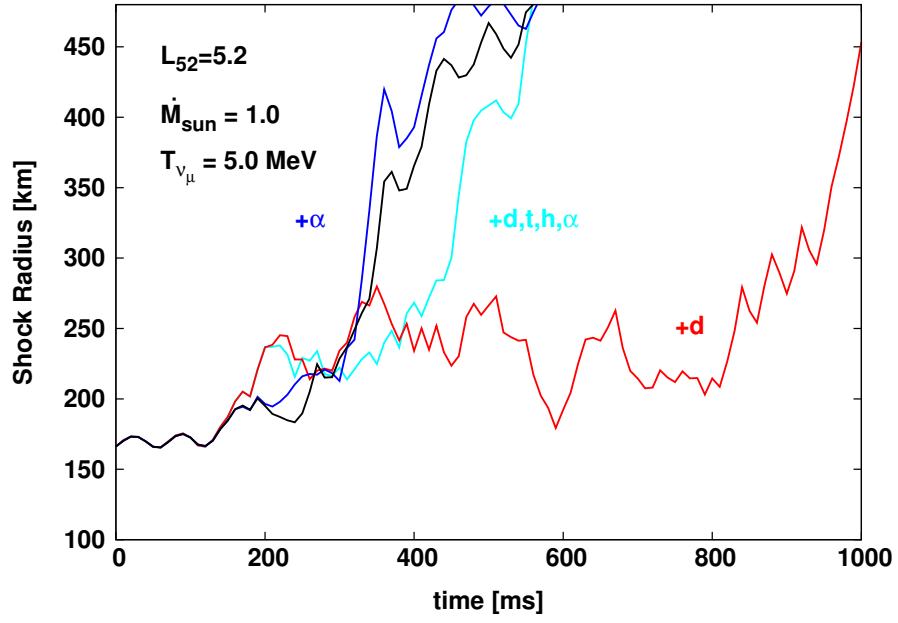


Fig. 11.— The time evolutions of the average shock radii for the models with the heating of all light nucleus (cyan line), only deuterons (red line), only alpha particles (blue line) and no light nuclei (black line). The temperature of  $\nu_\mu$  is  $T_{\nu\mu} = 5 \text{ MeV}$  and the luminosity and mass accretion rate are  $L_{52} = 5.2$  and  $\dot{M}_{\text{sun}} = 1.0$ , respectively.

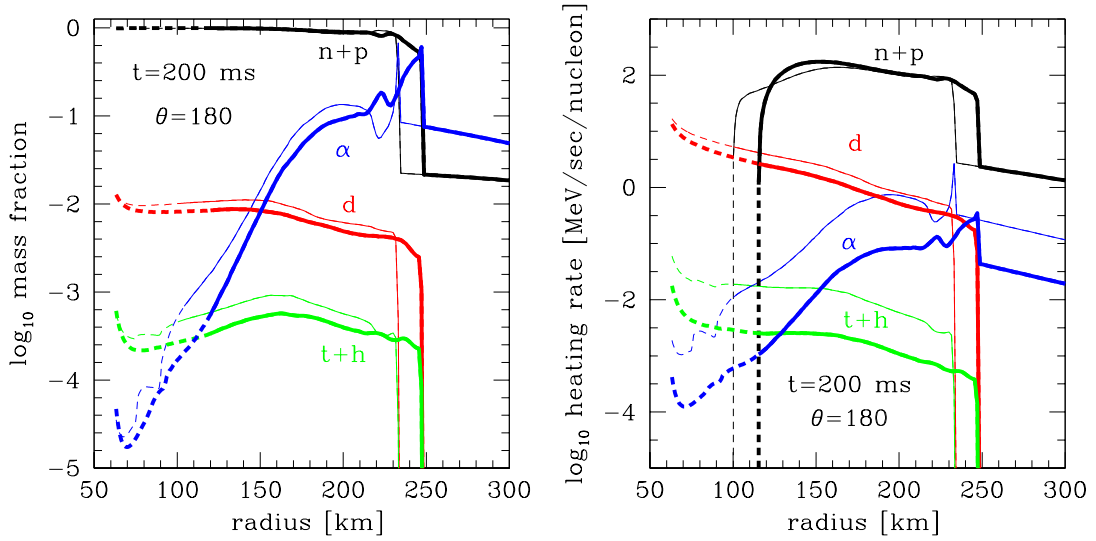


Fig. 12.— The mass fractions (left panel) and heating rates per baryon (right panel) along the radial ray with  $\theta = 180^\circ$  at  $t = 200$  ms for  $T_{\nu\mu} = 5$  MeV (thick lines) and 10 MeV (thin lines). The thin lines are just the same as those in the left panels of Fig 9 and the notations of lines are also identical to those in Fig. 9.

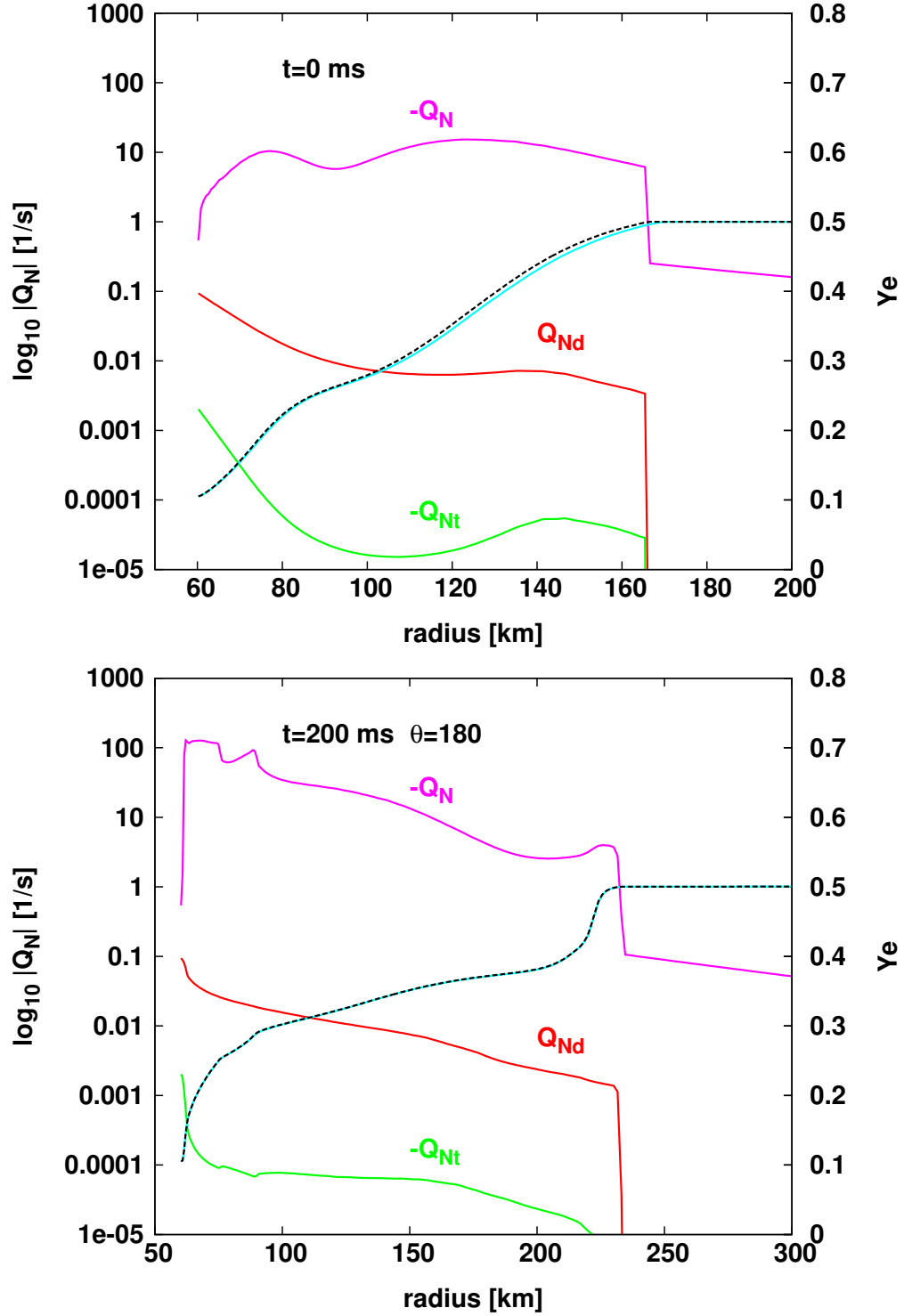


Fig. 13.— The electron fractions (black dotted line) and the absolute values of  $Q_N$  (magenta lines),  $Q_{Nd}$  (red solid lines) and  $Q_{Nt}$  (green solid lines) at  $t = 0$  and  $200$  ms along the radial ray with  $\theta = 180^\circ$ . See the text for the definitions of  $Q_N$ ,  $Q_{Nd}$  and  $Q_{Nt}$ . The electron fractions obtained with  $Q_{Nd} = Q_{Nt} = 0$  are also shown by the cyan solid lines.